

VIP Very Important Paper

Sulfur-Composites Derived from Poly(acrylonitrile) and Poly(vinylacetylene) – A Comparative Study on the Role of Pyridinic and Thioamidic Nitrogen

Julian Kappler,^[a] Sina V. Klostermann,^[b] Pia L. Lange,^[c] Michael Dyballa,^[d] Lothar Veith,^[e] Thomas Schleid,^[c] Tanja Weil,^[e] Johannes Kästner,^[b] and Michael R. Buchmeiser^{*[a]}

Sulfurized poly(acrylonitrile) (SPAN) is a prominent example of a highly cycle stable and rate capable sulfur/polymer composite, which is solely based on covalently bound sulfur. However, so far no in-depth study on the influence of nitrogen in the carbonaceous backbone, to which sulfur in the form of thioketones and poly(sulfides) is attached, exists. Herein, we investigated the role of nitrogen by comparing sulfur/polymer composites derived from nitrogen-containing poly(acrylonitrile)

(PAN) and nitrogen-free poly(vinylacetylene) (PVAc). Results strongly indicate the importance of a nitrogen-rich, aromatic carbon backbone to ensure full addressability of the polymer-bound sulfur and its reversible binding to the aromatic backbone, even at high current rates. This study also presents key structures, which are crucial for highly cycle and rate stable S-composites.

Introduction

With the changes in primary energy production that entails the substitution of fossil sources by regenerative ones, the demand for batteries with high gravimetric and volumetric energy density is growing rapidly.^[1] Conventional lithium-ion batteries (LIBs) are approaching their theoretical energy density limits; consequently, the further development of *post*-lithium-ion batteries becomes inevitable.^[2] The high theoretical capacity of sulfur (1672 mAh/g), its low toxicity and very low price make it a promising candidate as cathode material in conversion batteries. Combination with metallic lithium as anode material offers access to Li–S batteries, which are known to possess a

high theoretical gravimetric energy density of up to 2510 Wh/kg, with theoretical cell capacities of up to ≈ 1167 mAh/g – much higher compared to conventional LIBs.^[3] However, practical applications are limited due to fast aging of this battery type, mainly related to a constant loss of active material by migration of the intermediary polysulfides, formed upon reduction, to the anode – usually referred to as the „polysulfide (PS) shuttle“. Another issue is related to the density differences between α -S₈ ($\rho = 2.07$ g/cm³) and its discharge product Li₂S ($\rho = 1.66$ g/cm³). This gives rise to volume contraction and expansion effects, ultimately resulting in high mechanical stress within the cathode during charge and discharge.

One concept that is frequently chosen to alleviate cell aging via the PS-shuttle is the embedment of sulfur into porous carbon (PC) hosts.^[4] The possibility to tailor mass transport phenomena by the appropriate choice of surface parameters as one of the positive aspects is often drawn into shadow by complex synthetic protocols of these PCs. Furthermore, for optimum performance, high specific surface areas and large pore volumes are necessary for high sulfur loadings along with the ability to buffer volume contraction and expansion within the pores.^[5] Another drawback of these sulfur/PC composites is the fact that electrons have to cross one more interface to address the embedded S upon reduction in comparison to systems, in which sulfur is covalently attached to a composite and in which both, the carbon-matrix and the chemically bound sulfur, are within the same phase. An alternative, vividly discussed concept to overcome the challenge of fast aging via the PS-shuttle is therefore to chemically bind sulfur to a suitable matrix.^[6] Both, a high addressability of the bound sulfur even at high C-rates and a certain polarity of the matrix to facilitate the physical interaction with the polysulfides would be desirable. Detailed investigations that link defined microstructures of such composites to their electrochemistry are still scarce in this field of research.


[a] J. Kappler, Prof. Dr. M. R. Buchmeiser
Institute of Polymer Chemistry
University of Stuttgart
Pfaffenwaldring 55, 70569 Stuttgart (Germany)
E-mail: michael.buchmeiser@ipoc.uni-stuttgart.de


[b] S. V. Klostermann, Prof. Dr. J. Kästner
Institute of Theoretical Chemistry
University of Stuttgart
Pfaffenwaldring 55, 70569 Stuttgart (Germany)

[c] P. L. Lange, Prof. Dr. T. Schleid
Institute of Inorganic Chemistry (IAC)
University of Stuttgart
Pfaffenwaldring 55, 70569 Stuttgart (Germany)

[d] Dr. M. Dyballa
Institute of Technical Chemistry
University of Stuttgart
Pfaffenwaldring 55, 70569 Stuttgart (Germany)

[e] Dr. L. Veith, Prof. Dr. T. Weil
Max-Planck-Institute for Polymer Research
Ackermannweg 10, 55128 Mainz (Germany)

 Supporting information for this article is available on the WWW under <https://doi.org/10.1002/batt.202200522>

 © 2023 The Authors. Batteries & Supercaps published by Wiley-VCH GmbH. This is an open access article under the terms of the Creative Commons Attribution License, which permits use, distribution and reproduction in any medium, provided the original work is properly cited.

A very prominent example of a sulfur/polymer-composite that shows the aforementioned positive characteristics of composites bearing covalently bound sulfur is sulfurized poly(acrylonitrile) (SPAN), which is prepared via the thermal conversion of PAN in the presence of elemental sulfur. Since its discovery in 2002 by Wang et al., SPAN experienced a steadily growing interest in its chemical composition.^[7] The use of a broad scope of analytical techniques allowed for elucidating various structural key features of SPAN and led to a clearer picture of its structure.^[8] Thus, the exothermic cyclization of the nitrile groups together with concomitant sulfur-incorporation results in a carbonaceous, highly nitrogen-rich composite with a nitrogen content of ca. 14 wt%, to which sulfur is attached in form of (enolic) thioamides, forming N–C–S_x moieties. Properties such as a high rate capability, high cycle stability and compatibility with carbonates-based electrolytes are unique for the SPAN-composite and unusual for other sulfur-containing cathode materials.^[9]

Ever since, both the structure and morphology of SPAN and its composites have been optimized. Tailoring the macroscopic properties of SPAN-cathodes has been achieved through the usage of monolithic,^[10] fiber^[11] or particulate poly(acrylonitrile) (PAN) precursors with different molecular weights,^[12] which resulted in a unique electrochemical performance of SPAN composites and the resulting electrodes, respectively. Concepts to hierarchically design free-standing fibrous SPAN-cathodes were developed, too, and even offered access to stable Li-SPAN batteries in ether-based electrolytes, which are otherwise prone to aging via the *polysulfide shuttle mechanism*.^[13] The chemical composition of SPAN was further optimized by tweaking the sulfurization temperature as well as the vapor pressure^[14] during sulfurization or by doping SPAN with Se,^[15] Te^[16] or I.^[17] The resulting *eutectic accelerators* allow for faster kinetics of the solid-solid conversion during redoxing. Upscaling of SPAN-based cathodes to pouch cell formats has been realized, too, allowing for specific discharge capacities up to 1000 mAh/g_{sulfur} over 100 cycles at 0.5 C (C=C-rate).^[18] The specific capacities up to 1500 mAh/g_{sulfur} at discharge rates up to 10 C underline the superior performance of this composite and are unique amongst sulfur-based cathodes.^[19] Finally, the high electrochemical stability of SPAN towards a great variety of chemically different electrolytes also led to its successful implementation into other cell systems such as Mg–S,^[20] Na–S,^[21] K–S^[22] and Al–S^[23] cells. However, a full molecular understanding of SPAN's unique properties, especially how its electrochemical stability towards carbonates, the high rate and cycle stability are linked to the covalent fixing of sulfur to the carbonaceous backbone, is missing to date and can only be achieved through comparative studies of model systems.

A recent review already emphasizes the exceptional behavior of nitrogen-containing composites for use in Li–S batteries.^[6a] Indeed, many of the above-mentioned, unique properties of SPAN seem to be connected to the presence of nitrogen in the sulfur-containing carbonaceous matrix. We, therefore, screened and identified the most important differences between nitrogen-containing and nitrogen-free cathodes

containing covalently bound sulfur that are responsible for longevity and a high rate capability.

Results and Discussion

Thermal behavior, reactivity and sulfur-uptake of the precursor polymers

Thermal treatment of PAN leads to cyclization of the nitrile groups in the polymer chain to form conjugated, ladder-like structures often referred to as cyclized PAN (cPAN).^[24] If this reaction is performed under oxidative conditions, e.g., in air, the cPAN backbone incorporates O-containing functional groups, amongst these mainly hydroxyl- and ketone-groups.^[25] Similarly, thermal treatment of PAN in the presence of sulfur as oxidative reagent results in an analogous reaction, forming a composite referred to as SPAN.^[7a] SPAN's most relevant structural motifs are polysulfides bound to the carbonaceous (aromatic) matrix via (enolic) thioamides.^[8a–c] To reveal the role of nitrogen, an SPAN-analogous composite based on a polymer with similar cyclization behavior as PAN was chosen. Poly(vinylacetylene) (PVAc) fulfills these criteria and was therefore already used as a precursor for carbon fibers.^[26] The polymerization of vinylacetylene, however, is impeded by the high volatility of the monomer, its brisance as highly unsaturated C₄-hydrocarbon and the strong exothermic reaction during cyclization, which was reported to result in explosions.^[27] Therefore, an alternative synthetic route to poly(vinylacetylene), which entails the preparation of trimethylsilylvinylacetylene (TMSVAc), its polymerization in bulk followed by removal of the TMS-group utilizing a polymer-analogous reaction, was developed. By optimizing the deprotection protocol we could achieve a degree of deprotection of 99.7%, allowing for the synthesis of virtually pure PVAc as the pseudo-copolymer **P2** (Figure 1). To the best of our knowledge, the aforementioned conversions are by far the highest reported in the literature so far.^[28] Differential scanning calorimetry (DSC) measurements of the precursor polymers confirm the successful thermally-induced cyclization of PVAc (Figure 2a). Both, PAN and PVAc, show a highly exothermic cyclization with a lower T_{onset} for PVAc (204 °C) compared to PAN (283 °C). However, the overall cyclization window is broader for PVAc though the exothermicity is much more pronounced in PVAc (1400 J/g) compared to PAN (440 J/g). Thermogravimetric analysis (TGA) revealed a similar mass loss for PVAc and PAN with residual masses of 29% (PAN) and 24% (PVAc) after heating to 1000 °C, which again underlines that both polymers are capable of building a stable, carbonaceous structure upon thermal treatment – a prerequisite for using these polymers as precursors for sulfurization at elevated temperatures.

Notably, the sulfur-uptake of PVAc was much lower than for PAN under the same reaction conditions (550 °C, 5 h, N₂). However, optimization of the synthetic protocol via introduction of a longer low-temperature plateau (150 °C) and dynamic vacuum (10^{−3} mbar) to facilitate hydrogen-elimination resulted in SPVAc with a sulfur-content comparable to the one of SPAN

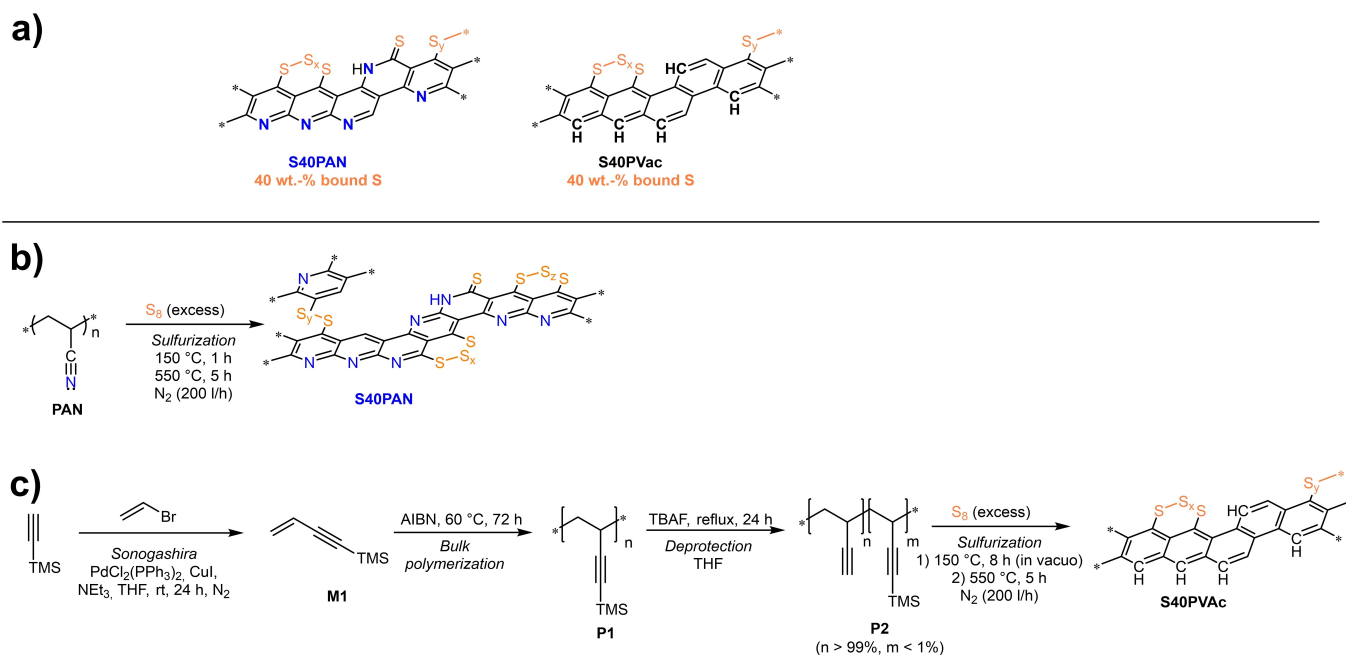


Figure 1. a) Model structures SPAN and SPVac composites and the synthetic routes to b) S40PAN and c) S40PVac.

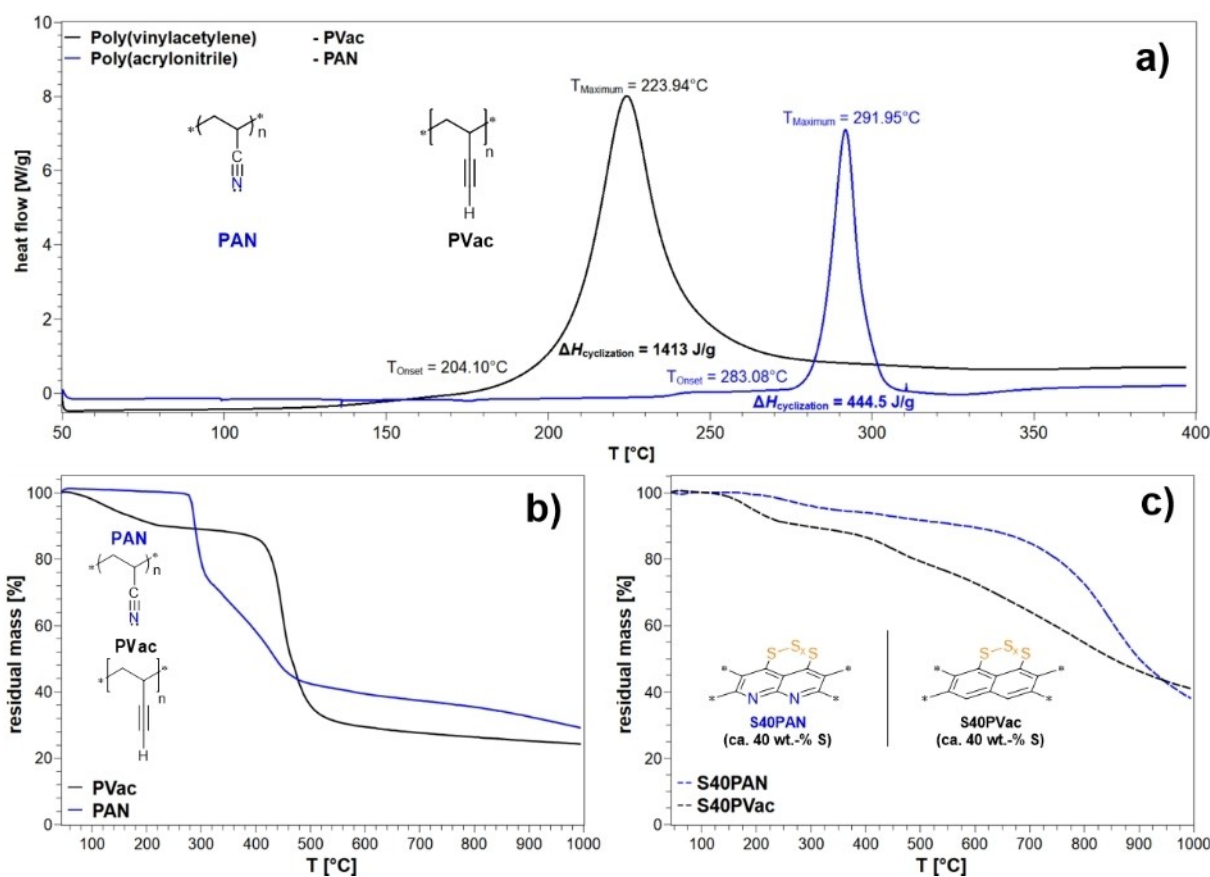


Figure 2. a) DSC curves of the precursor polymers, b) TGA curves of PAN and PVac and c) TGA curves of S40PAN and S40PVac.

(40 wt%). The application of a dynamic vacuum during synthesis was indeed found to be crucial since the sole extension

of the 150 °C plateau under atmospheric nitrogen pressure only resulted in SPVac with a low sulfur content (32.5 wt% S,

Table S1). The sulfurized composites derived from the polymers PAN and PVac (P2) are referred to as S40PAN and S40PVac, respectively, to indicate the comparable sulfur-content of both composites. It is noteworthy that PVac shows a low T_{onset} for sulfur incorporation while PAN showed no S-uptake at 150 °C (8 h) as determined by a control experiment (< 0.2 wt% S). TGA-measurements of S40PAN and S40PVac revealed a strong binding of sulfur to the matrix as illustrated by a mass loss of less than 20 wt% up to 500 °C in both composites (Figure 2c). This is in stark contrast to conventional S/C composites, in which the mass loss stemming from S-evaporation is often nearly quantitatively completed at approx. 400 °C due to the high volatility of elemental sulfur.^[29]

Molecular and morphological characteristics of SPAN, SPVAc and the resultant cathodes

Differences in the electrochemical behavior of SPAN and SPVAc are linked to the differences in molecular structure and morphology of the sulfurated carbonaceous backbone. SPAN has been reported to possess covalently bound sulfur in form of (enolic) thioamides and polysulfides, in which the sulfur is mainly present in the form of short S_x chains with $x \leq 7$.^[8a-c,11] The ^1H - ^{13}C cross-polarization-magic-angle-spinning nuclear magnetic resonance (CP MAS NMR) spectra (Figure 3a, b) confirmed the formation of a pyridinic/arylic backbone in S40PAN and of an arylic backbone in S40PVac. In S40PAN, arylic/pyridinic carbons bound to H and S were observed at $\delta = 127.9$ ppm and 118.8 ppm respectively. The intense signal at $\delta = 150$ ppm in S40PAN is assignable to carbons in close vicinity to nitrogen, i.e. to pyridine and thioamide moieties. In S40PVac, arylic carbons bound to H and S were observed at $\delta = 137$ ppm and 127.7 ppm. The absence of any aliphatic carbons and the sole presence of aromatic carbons is again consistent with our hypothesis that both, PAN and PVac, undergo a cyclization reaction in the presence of sulfur as oxidant and a subsequent aromatization during sulfurization at elevated temperatures. In line with that, S40PVac showed no signals for residual internal alkyne groups.

The most prominent signals in the ATR-FT-IR spectra of PAN and PVac (Figure 3c, d; dashed lines, Figure S20) were the $\text{C}\equiv\text{N}_{\text{PAN}}$ stretching at 2250 cm^{-1} , $\text{C}\equiv\text{C}_{\text{PVac-H}}$ (internal) at 2150 cm^{-1} , $\text{C}\equiv\text{C-H}_{\text{PVac}}$ (terminal) at 3340 cm^{-1} , C-H_{PAN} at $2940\text{--}2865\text{ cm}^{-1}$ and C-H_{PVac} at $2970\text{--}2840\text{ cm}^{-1}$. In the IR-spectra of the corresponding sulfurized composites S40PAN and S40PVac (Figure 3c, d; solid lines), broad absorption bands below 1650 cm^{-1} were found for both, S40PAN- and S40PVac, indicating arylic (S40PVac and S40PAN) and pyridinic (S40PAN) $\text{C}=\text{C}$ and $\text{C}=\text{N}$ valence vibrations. In line with earlier reports, the band at 1500 cm^{-1} in S40PAN was assigned to the thioamide-group.^[8a] Unlike in PAN, S-binding to PVac occurs at the alkyne-side groups prior to cyclization with the terminal alkyne-proton as the most reactive site in the polymer. This was confirmed by IR-analysis and by the finding that gas evolution started already at 150 °C, which is below the cyclization onset-temperature (204 °C, Figure 2a).

This is in strong contrast to the sulfurization behavior of PAN, which did not show any sulfur uptake after heating to 150 °C as confirmed by a control experiment and in which the only protons available for H_2S formation are located in the polymeric backbone and require higher temperatures to react. IR-assisted analysis of the SPVAc composites confirmed that the low T_{onset} mainly stems from the highly reactive terminal alkyne protons in PVac (Figure S1). Thus, the characteristic stretching vibration of the terminal alkyne proton in PVac (3293 cm^{-1} ; Figure 3c, dashed line) strongly decreases in intensity after sulfurization for 8 h at 150 °C (Figure S1). Notably, the signals for the $\text{C}\equiv\text{C}$ bond (internal alkyne, 2113 cm^{-1} ; Figure 3c, dashed line) during the major sulfur-uptake prevail before complete cyclization occurs. Also, SPVAc composites obtained after further heating to 550 °C consistently showed high C:H ratios, indicating aromatization via the removal of hydrogen through the release of H_2S (Figure S2). X-ray diffraction (XRD) and Raman data suggest that the aromatic layers of the conjugated π -system, which is formed in the course of the cyclization reaction of PAN and PVac, are aligned in a turbostratic manner under π - π -stacking (Figure 3e, f).

The powder X-ray-diffractograms of S40PVac and S40PAN showed characteristic reflexes at $2\theta = 19.3^\circ$ (S40PAN) and 19.6° (S40PVac), respectively. These reflexes can be attributed to the d_{002} plane and are directly linked to interplane distances between the aromatic layers.^[30] According to Bragg's law, the interlayer distance was 1.8 Å (S40PAN) and 1.1 Å (S40PVac). The increased interlayer distance in S40PAN can be attributed to the structural disturbance by the pyridine nitrogens in the S40PAN backbone. No crystalline sulfur ($\alpha\text{-S}_8$) was detected; consequently, the presence of shorter, intercalated sulfur-allotropes can also be excluded since these would transform into $\alpha\text{-S}_8$ over time.^[31] The Raman-spectra confirm π - π -stacking due to the presence of the characteristic G- (1555 cm^{-1}) and D- (1380 cm^{-1}) bands (Figure 3f). The numeric intensity ratios between the G- and D-band deliver information about defects in carbonaceous materials.^[14,32] The I_D/I_G ratios for S40PAN (0.96) and S40PVac (1.0) were both close to unity, despite the absence of nitrogen in S40PVac.

Differences and similarities between S40PVac and S40PAN in terms of their binding states and functional groups were investigated by X-ray photoelectron spectroscopy (XPS, Figure 4). The N 1s spectrum of S40PAN was in agreement with the literature; mainly pyridinic (400 eV) and thioamidic (398.2 eV) structures were observed.^[8a] No residual nitrogen, e.g. from the tetrabutylammonium fluoride (TBAF) facilitated deprotection of P1 was found in the N 1s spectrum of S40PVac. In the C 1s spectra of S40PAN, signals that could be assigned to aromatic and aliphatic carbons (C-C/C-H , 284.8 eV), as well as to C-S (284.8 eV), C=N (286.5 eV) and C-O (285.6 eV) bonds were found. This assignment was made based on the assumption that the C-S and C-C/C-H bonds are represented by the same signal, as the differences in electronegativity between C and S are low. For S40PVac C-C/C-H , C-S (both at 284.8 eV) and C=O (286.9 eV) moieties could be identified. The broad peak at 286.9 eV in S40PVac is very likely related to oxidized surface carbon and is denoted C=O herein, however,

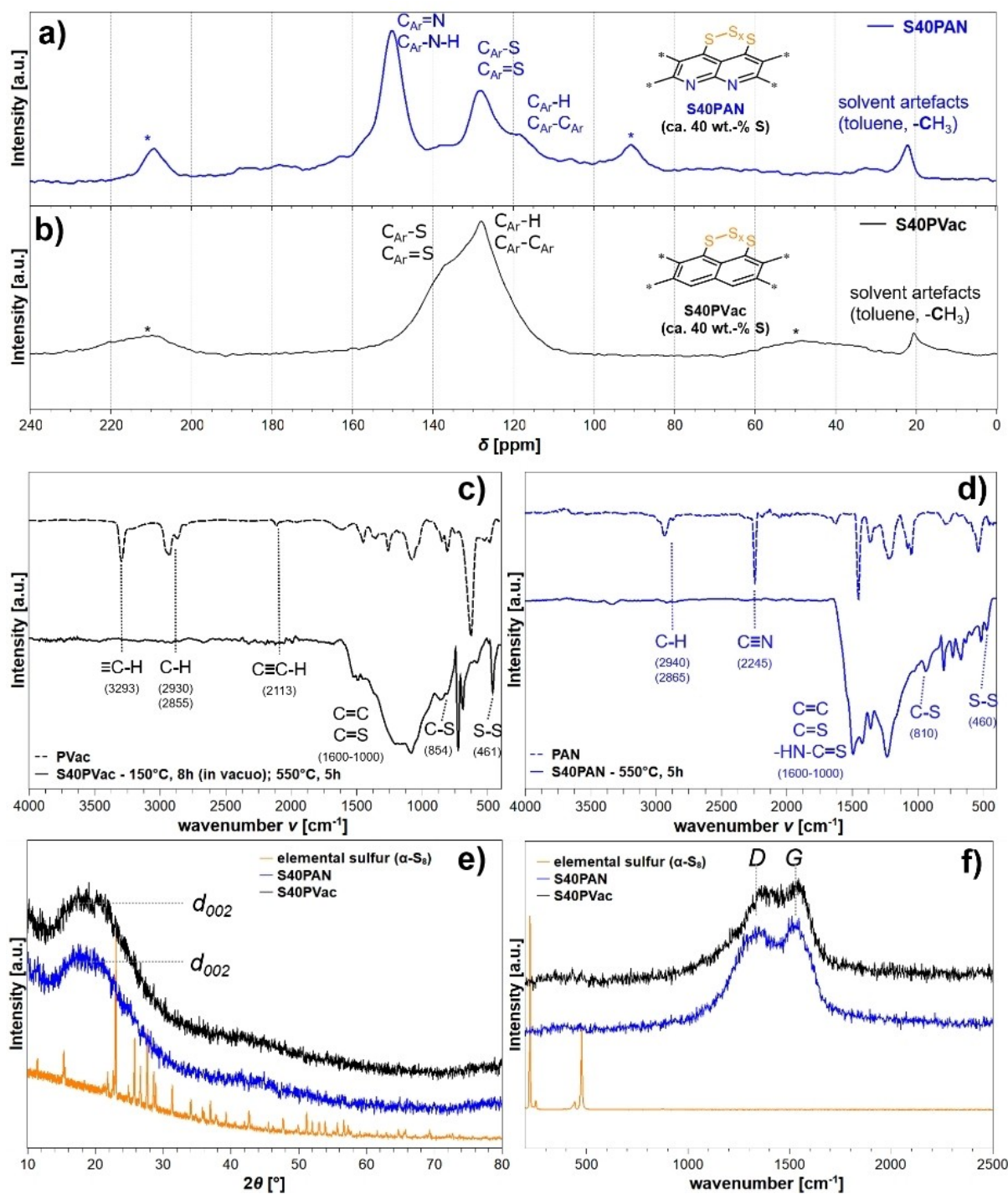


Figure 3. ^{13}C CP MAS NMR spectra of a) S40PAN and b) S40PVac. ATR-IR spectra of c) PVac-, and S40PVac-, and d) PAN- and S40PAN-composites. e) Powder X-ray diffractograms (Cu-K α) and f) Raman-spectra (Nd-YAG-laser, 532 nm) of elemental sulfur, S40PAN and S40PVac.

the broadness of the signals indicates that there is, beside the ketone groups, probably a variety of differently oxidized carbons present (e.g. in the form of carboxyl-groups).^[33] The high-resolution S 2p spectra of S40PAN indicate C–S and S–S bonds from sulfides and polysulfides at 163.6 eV ($\text{C}-\text{S}_x$, $\text{S}-\text{S}_x$ with $x \geq 0$) as well as thioamidic S at 161.7 eV ($-\text{NH}-\text{C}=\text{S}$, denoted $\text{C}=\text{S}$ herein), which is in line with reports published earlier.^[11] In S40PVac (poly)sulfidic ($\text{C}-\text{S}_x$, $\text{S}-\text{S}_x$ with $x \leq 0$;

163.9 eV) and thioketonic S ($\text{C}=\text{S}$; 161.7 eV) moieties were detected. Furthermore, a broad signal at 164.8 eV was assigned to oxidized S species ($\text{S}(=\text{O})_x$ where $x = 1-3$). Notably, significantly less sulfur in form of thioketones was found in S40PVac ($\text{C}=\text{S}$; relative area 5.4%) than in S40PAN ($\text{C}=\text{S}$; relative area 21.6%). We attribute this finding to the possibility of thioamide formation in PAN upon sulfur-incorporation, cyclization and through the addition reaction of H_2S to nitriles, which is known

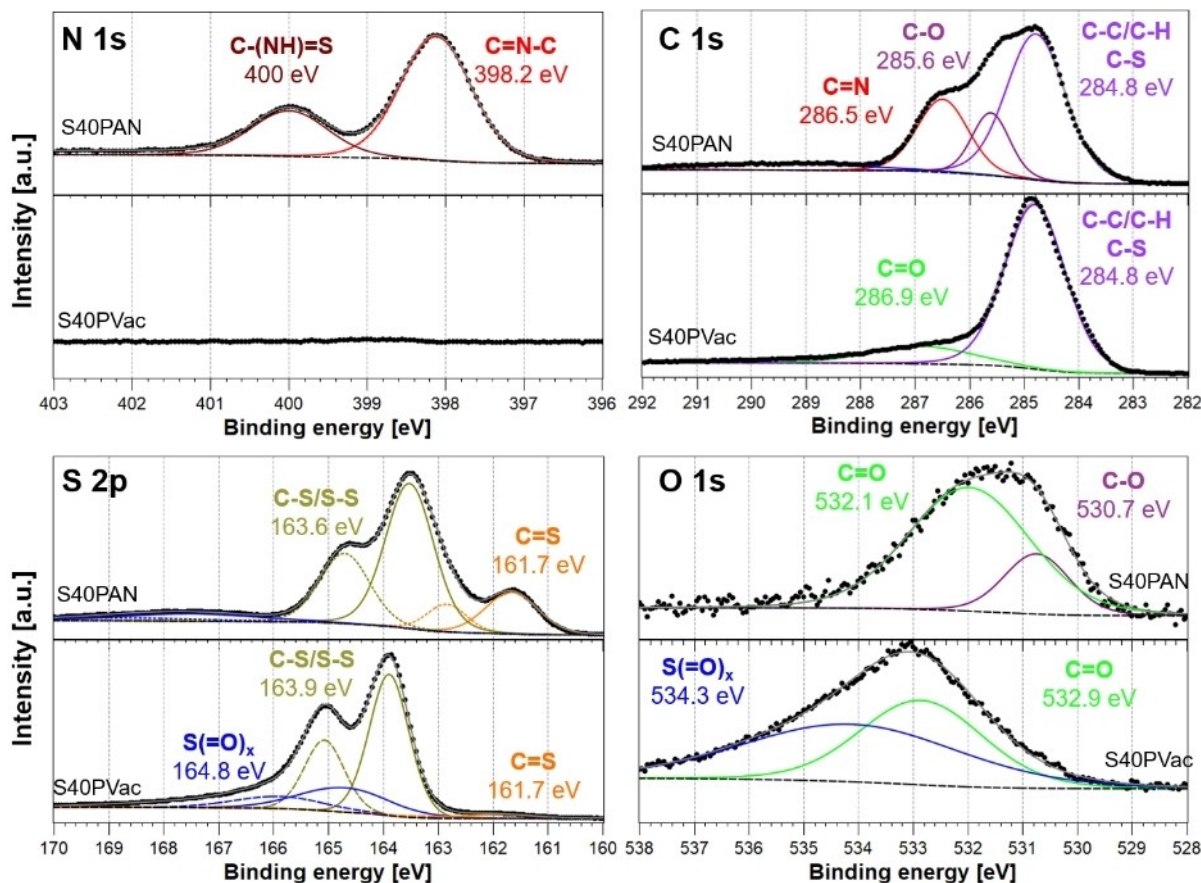


Figure 4. High-resolution XPS data of S40PAN (top panels) and S40PVac (bottom panels).

to be less preferred in their alkyne counterparts.^[34] Furthermore, the thioamide structure in S40PAN is more stabilized due to better electron density distribution in the thioamide than in nitrogen-free S40PVac and therefore thermodynamically favored.

XPS unveiled minor amounts of O at 531–534 eV, both in S40PAN and S40PVac. These can be ascribed to C=O, S(=O)_x, and C–O but could also be related to adsorbed water and oxygen and residual redox initiator, as well as to oxide layers on the indium-foil, which was used for sample preparation.^[35] Small amounts of Si could be detected in both, S40PAN and S40PVac, too, assignable to the common surface contaminant poly(dimethylsiloxane) (PDMS). To quantify residual trimethylsilane related to insufficient conversion of P1 into P2 (see Figure 1c), Si-values were determined by inductively-coupled plasma-optical emission spectroscopy (ICP-OES) and found to be low (0.3–0.5 wt%), which is consistent with the obtained ¹³C and ¹H NMR data for P2 and the low intensity of the Si 2s signals at 155.3 eV in the XPS data (Figure S3).

In S40PAN, time-of-flight secondary ion mass spectrometry (ToF-SIMS) allowed for identifying various C_aN_b⁻ and C_aN_bS_c⁻ clusters in the negative ion mode with $m/z \leq 180$. Signals at $m/z = 74$ (C₅N⁻) and 72 (C₆⁻) suggest the formation of benzene and pyridine units during the thermally-induced sulfurization of PAN (Figure S4). It is noteworthy that no fragments indicating N–S bond formation could be identified ($m/z = 47$, NS⁻), neither

in ToF-SIMS, nor in high resolution XPS. Again, the intense signals at $m/z = 58$ (NCS⁻) and 82 (NC₃S⁻) support thioamide formation in SPAN, as well as sulfur-incorporation in the α -position to the pyridinic nitrogen, leading to kinks in the otherwise linear carbon matrix (Figure S5). Similar effects could also be expected for S40PVac formation, but cannot be detected utilizing ToF-SIMS due to the lack of heteroelements in the composite. In S40PVac the major part of the secondary ions constituted of C_yS_x⁻ units (Figure S6). To investigate the average length of the S_x units in S40PVac and S40PAN, the normalized signal intensities for the S_x clusters were compared to the total ion signal (Table S2, Figure S7). Unsurprisingly, the intensities of the S_x-clusters decreased with increasing chain length such that especially signals for $x \geq 4$ were of low intensity. In direct comparison between S40PAN and S40PVac a similar distribution of the different S_x-clusters was observed with the highest intensities for S_x with $1 \leq x \leq 3$. In S40PVac a shift of the average S_x-clusters length to longer S_x-species was visible. Application of the activation protocol (150 °C, 8 h, 10⁻³ mbar) resulted in longer S_x-clusters in the S40PVac composite, since sulfur at these temperatures is mainly present in the form of longer S_x-units.^[6b,31a,36]

Morphological analysis using scanning electron microscopy (SEM) showed an inhomogeneous particle size distribution and similar particle shapes for both sulfur composites (Figure 5a₁, b₁). Exemplary SEM pictures of the S40PAN- and S40PVac-

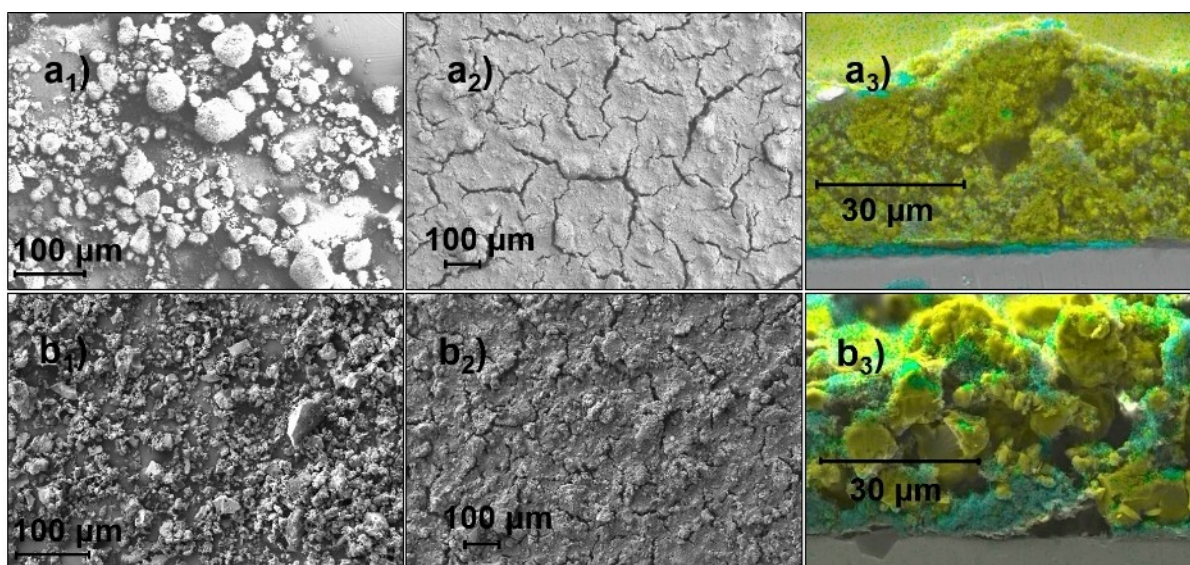


Figure 5. SEM images of a) S40PAN and b) S40PAN-based cathodes. Indices: 1) primary particles, 2) cathodes (top view) together with SEM-EDX images of the 3) cathode cross-sections (yellow: sulfur, aquamarine: fluorine). A wet coating thickness of 200 μm was applied. Cathode composition: S-composite: PVdF:SuperC65 = 70:15:15.

derived cathodes (Figure 5a₂, b₂) and SEM-EDX mapping of cathode components at the cross-section showed that both, S40PVac and S40PAN, were evenly distributed along the cross-section, though with overall larger particle agglomerates in S40PVac than in S40PAN (Figure 5a₃, b₃). In some domains the cross sectional images revealed an accumulation of poly(vinylidene fluoride) (PVDF) either at the top of the cathode or at the current collector-cathode interface, an effect which seems to be characteristic for PVDF-containing electrodes after applying higher drying temperatures (> 30 °C).^[37]

In order to suppress the influence of tortuosity and link differences in cycle stability to the molecular properties of the active materials, the comparison between the two active materials focused on low current rates (≤ 1 C).

Electrochemistry of S40PAN- and S40PVac-based cathodes

In view of the very similar molecular structures of S40PVac and S40PAN, a comparison between these two cathode materials in terms of electrochemical performance seemed most appropriate. 1 M Lithium(bistrifluoromethylamide) (LiTFSI) in DME:DOL (1:1; DME = 1,2-dimethoxyethane, DOL = 1,3-dioxolane) and 1 M LiPF₆ in DEC:EC (1:1 + 10 wt% FEC; DEC = diethyl carbonate, EC = ethylene carbonate, FEC = fluoroethylene carbonate) were chosen as ether- and carbonate-based model electrolytes, respectively. Cyclic voltammetry (CV) revealed a solvent-dependent redox behavior in both, S40PAN- and the S40PVac-based cathodes (Figure 6). In the ether-based electrolyte (Figure 6, left), the CVs showed a distinct decrease in the current density during cycling, likely stemming from a loss of active material.

A typical feature of sulfur-based cathodes in Li-S batteries is the appearance of a reduction peak at 2.35–2.4 V (vs. Li/Li⁺) in

ether-based electrolytes, which can be ascribed to the reductive ring opening of cyclic α -S₈, a step that is fast in kinetics due to the formation of soluble species of the general formula Li₂S_x ($x=6-8$).^[38] To our surprise, S40PAN and the S40PVac composites showed a comparable behavior despite the absence of elemental sulfur (α -S₈) and the sole presence of covalently bound S_x-chains. This suggests a conversion mechanism similar to the one in pure S₈-based active materials. The reduction signal at 2.4 V is followed by a broader reduction range between 2.1 V and 1.2 V, which we attribute to the conversion of longer S_x-species to Li₂S₂ and Li₂S, again, in similarity to α -S₈-based cathode materials.

In the carbonate-based electrolyte, however, a strong shift of the reduction signals to lower potentials with increasing number of cycles was observed for all composites (Figure 6, right). In S40PAN, the reduction signals at 1.8 V and 1.5 V, respectively (Figure 6, top right), indicate that the carbonate-based electrolyte facilitates a direct solid-solid transition of bound PSs into Li₂S without the appearance of longer PSs as intermediates – a finding which is unique for the SPAN composite in carbonate-based electrolytes and in contrast to the results using an ether-based electrolyte.^[39] In the S40PVac composites, a single reduction signal at 1.3–1.4 V was found (Figure 6, bottom right), suggesting that by switching to carbonate-based electrolytes a direct solid-solid conversion of LiPSs is induced and the formation of longer LiPSs is thereby suppressed – a feature which was verified for S₈-based cathodes, too.^[40]

Galvanostatic cycling (Figures 7 and S22) also showed that both reversibility and the redox mechanism were solvent-dependent, confirming the findings discussed above. A model S/C composite generated by high energy ball milling of acetylene black and elemental sulfur (wt./wt. – 1:1) was used to investigate the benefits that originate from the covalent

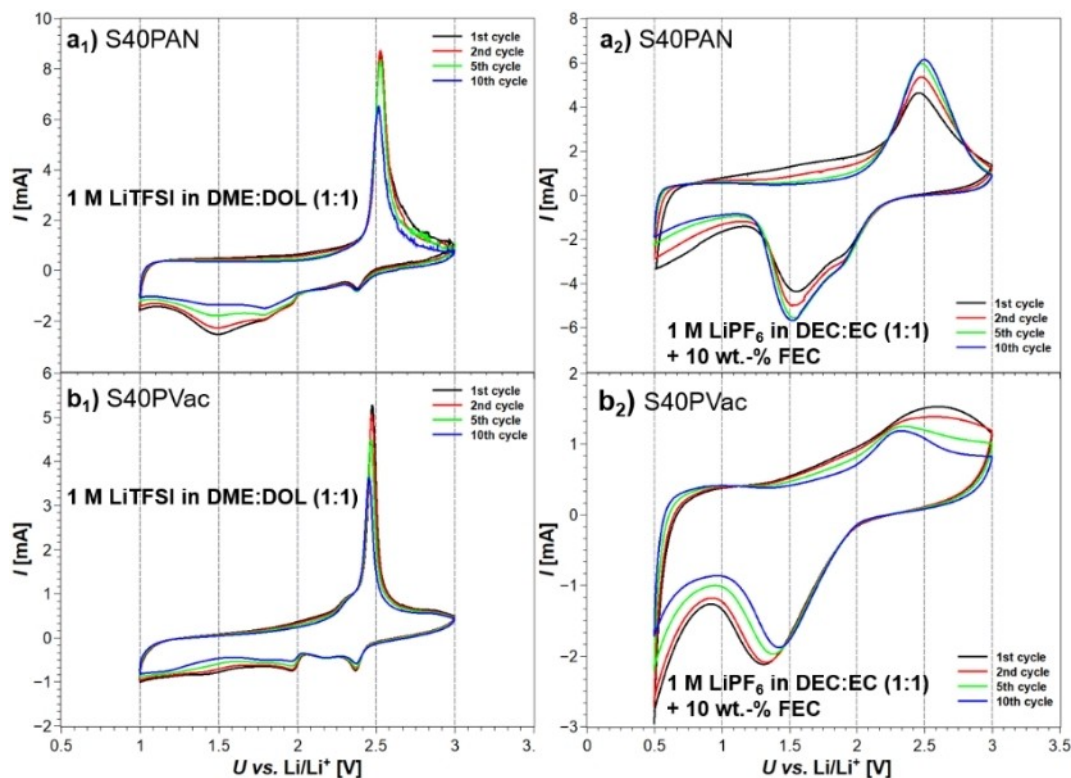


Figure 6. CVs of S40PAN and S40PVac in an ether- (1 M LiTFSI in DME:DOL (1:1); left) and carbonate-based (1 M LiPF₆ DEC:EC (1:1) + 10 wt.% FEC; right) electrolyte (all vs. Li/Li⁺).

binding of S to a carbon matrix similar to that of the S40PVac composite. Impressively, S40PAN outperformed the S40PVac and model S/C composites in terms of sulfur addressability in both electrolytes. Especially in the carbonate-based electrolyte, the S40PAN-based cathodes outperformed S40PVac-based cathodes independently of the applied current rates (Figure 7a). The initial capacity of both composites was much higher in comparison to the discharge capacity in the subsequent cycles, a phenomenon which was ascribed to overreduction of the carbon backbone in S40PAN. According to the similarity found in S40PVac-based cathodes, we conclude that the same is valid for S40PVac. Nevertheless, after the initial capacity loss, S40PAN retains a high reversible addressability exceeding 1100 mAh/g_{Sulfur} at 1 C (0.7 mA/cm²) over more than 1000 cycles at high coulombic efficiencies (CE) (>99%, Figure 7b) while S40PVac shows severe capacity degradation within the first 20 full cycles (Figure 7a).

An in-depth analysis of the potential profiles of S40PAN, S40PVac and the model S/C composite revealed that S40PAN shows a quite constant decrease in potential during discharge starting from 2.1 V (vs. Li/Li⁺), caused by the continuous release of Li₂S₂ and Li₂S (solid-solid conversion) without the appearance of long PS intermediates (Figure S8a). This is in contrast to the findings for S40PVac- and the model S/C-based cathodes, which both showed a characteristic plateau during discharge at 2.4 V (vs. Li/Li⁺, Figure S8b and c). Our findings strongly suggest that this unique redox mechanism of S40PAN is critically influenced by the presence of nitrogen in the carbona-

ceous backbone. A weaker C-matrix-PS-interaction, as found in the S40PVac material, could lead to easier migration of PSs in the electrolyte phase, followed by various parasitic side reactions that are already reported in conventional, sulfur-based cathode materials utilizing carbonates as electrolytes.^[41] Rate tests of S40PAN- and S40PVac-based cells confirmed a higher rate capability of S40PAN-based cathodes, likely owing to the more conductive nature of the carbon backbone. Systematic studies verified the improved electronic conductivity of SPAN through embedding nitrogen in the form of pyridine and pyrrol moieties into the carbonaceous matrix.^[42]

Matrix-Li₂S interactions for reduced S40PVac and S40PAN intermediary structures were calculated using density functional theory (DFT) to provide further evidence for the importance of a nitrogen-rich carbon matrix. A more than four-fold stronger interaction between Li₂S and S40PAN in its reduced form was found in comparison to S40PVac (Figure 8a₁ and b₁). We postulate that the nitrogen-rich environment in S40PAN actively facilitates Li₂S nucleation, which is less favorable in S40PVac. Due to the lower interaction energy between Li₂S and S40PVac the migration of LiPSs into the electrolyte during discharge becomes also more likely, in line with the observations in the potential profile upon discharge of S40PVac, in which plateaus for a solid-liquid transition were observed even in the carbonate-based electrolyte. This hypothesis is in line with electronic impedance spectroscopy (EIS) data for Li-S40PAN full cells at 100% SOC (Figures 8 and S9). The Nyquist plots of Li-S40PAN cells showed a strong initial

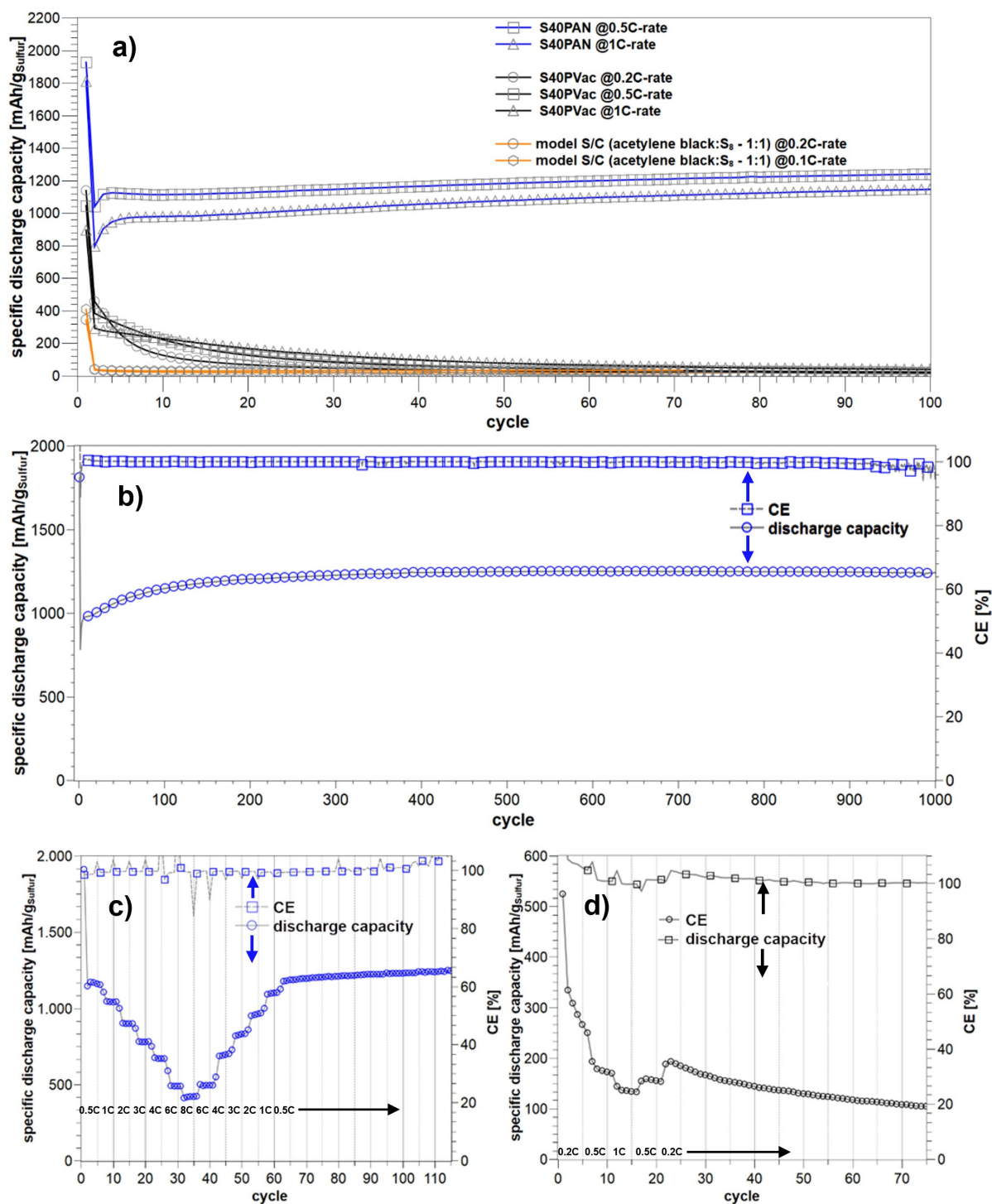


Figure 7. a) Galvanostatic cycling of Li||S40PAN, Li||S40PVac and Li||S/C cells at discharge rates between 0.1 and 0.5 C; b) long-term stability test of a Li||S40PAN cell at 1 C; c) rate capability of a Li||S40PAN cell between 0.5 and 8 C and d) rate capability of a Li||S40PVac cell between 0.2 and 1 C in 1 M LiPF₆ in DMC:EC (1:1) + 10 wt.-% FEC (1–3 V vs. Li/Li⁺).

decrease in the full cell impedance due to the generation of a fresh Li-surface. In the following cycles, a constant full cell impedance was observed and confirmed the high reversibility of the redox behavior seen in (Figure 8b). The determination of static contact angles using demin. H₂O as analyte suggests that this aforementioned hypothesis can at least partially be attributed to differences in polarity between the two active

materials (Figure S10). S40PAN-derived cathodes ($\theta_{\text{static}} = 104.5^\circ$) all showed better wetting properties in comparison to S40PVac-derived cathodes ($\theta_{\text{static}} = 111.2^\circ$).

The results shown herein strongly suggest that covalent binding of sulfur to a polymeric matrix is an important concept to generate a stable electrochemistry. In addition, a nitrogen-rich environment in close vicinity to bound PSs, however, is

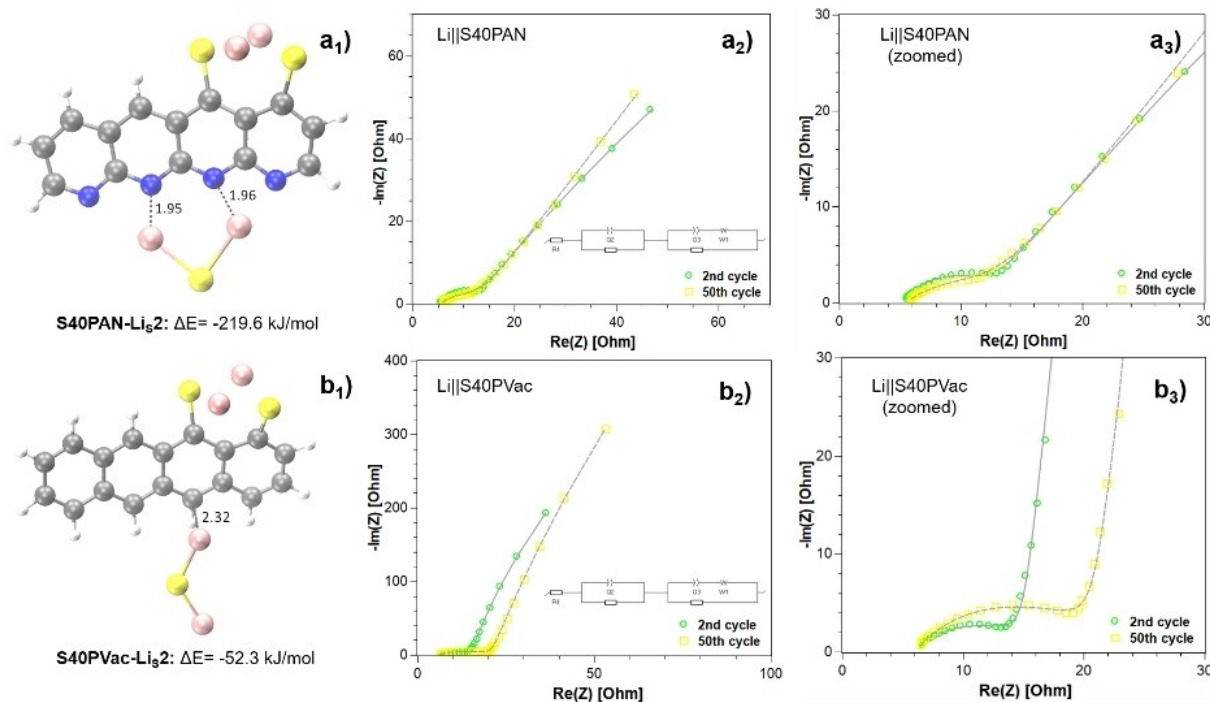


Figure 8. a, b₁) Optimized geometries of reduced S40PAN and S40PVac and their calculated interaction energies with Li₂S and a, b₂) full cell impedance measured by EIS of Li||S40PAN and Li||40PVac cells at 100% SOC after the 2nd and 50th cycle (0.5 C) using 1 M LiPF₆ in DMC:EC (1:1) + 10 wt% FEC and a, b₃) zoomed view.

also of key importance to facilitate a redox mechanism that inherently alleviates the PS-shuttle mechanism by the sole release of solid intermediates during discharge.

To further support these findings, ex situ XPS was applied to the derived cathodes after initial discharge and subsequent charge to monitor the differences in the binding states of S and to investigate the fast capacity fading of S40PVac-based cathodes (Figure S11). An emphasis was put on the analysis of the high-resolution S 2p spectra since in these only minor or no interference with signals from the polymeric binder, a potential SEI or residual solvents was expected. A first qualitative observation in the spectra of both S40PAN- and S40PVac-based cathodes was that any signals of bound sulfur are shifted towards higher binding energies compared to the pristine S40PAN and S40PAN samples. A similar effect was described by Eng et al. and has been attributed to the influence of the binder matrix, in particular the high negative charge density on characteristic molecular units of this matrix.^[43] In analogy to the ground state of the pristine material itself (Figure 4), signals for the C–S_x (164.5 eV) and C=S (162.5 eV) bonds can be assigned in S40PAN. In the fully discharged state, the presence of Li₂S (161.7 eV) was assigned as the discharge product. A slight shift of the binding energy to 161.7 eV compared to the literature value^[44] (160.8 eV) can be attributed to the binder matrix as well as to a strong interaction of the lithiated cPAN matrix with Li₂S (see DFT calculation above). Li thiolate groups remaining on the cPAN were identified according to Jin et al. (C–S[−]Li⁺, 163.0 eV).^[45] It can be further assumed that the excess capacitance detected for S40PAN in the initial cycle also reduces/lithiates the C matrix (Figure S21). We postulate there-

from that the signal at 165.1 eV can be assigned to C–S_x bonds that were not fully addressed in the course of cyclization, but are shifted toward higher binding energy (C–S_x^{*}) due to the high negative charge density caused by the reduced C matrix. In the fully charged state, a restoration of the S40PAN basic structure becomes evident, which is also supported by nearly equivalent ratios of the C–S_x (164.6 eV) and C=S (162.3 eV) bonds compared to the initial state. For the S40PVac cathodes, the presence of C=S (162.5 eV), C–S_x (164.5 eV), and S(=O)_x (165.3 eV) moieties was found. It can be assumed that specifically the oxidized sulfur species barely participate in the electrochemical reaction; the following discussion therefore focuses essentially on the participation of the thioketone and sulfide moieties.

In analogy to the arguments used for the S40PAN material, it is also reasonable to assume for S40PVac that a substantial part of the C–S_x bonds is electrochemically unaddressed due to the high negative charge density of the C-matrix after the initial discharge. These are also indexed here by C–S_x^{*} and localized at nearly equivalent binding energy as in S40PAN (C–S_x^{*}: S40PAN - 165.1 eV; S40PVac - 165.0 eV). We postulate that the signal located at 163.0 eV, again as in S40PAN, can be assigned to C–S[−]Li⁺ bonds, possibly superimposed by the presence of long-chain lithium polysulfides through incomplete reduction. It is known that lithium as well as other alkali metal sulfides and polysulfides exhibit signals in the S 2p spectrum that gradually appear at higher binding energies with increasing chain lengths.^[44] In the charged state, the S40PVac cathode displays three binding species in analogy to the initial state, which were again assigned to C=S (162.6 eV), C–S_x (164.7 eV)

and oxidized S species (165.9 eV). Compared to the initial state, a slight shift towards higher binding energies was observed throughout, possibly due to an overall slightly higher ionic character (e.g., due to overreduction of the C-matrix) of the reduced S40PVac material compared to the pristine state. Significantly, however, the signal of the C–S_x bonds was drastically reduced in relative intensity compared to the remaining signals during the initial cycle. It can thus be assumed that a substantial part of the bound sulfur migrates into the electrolyte phase already in the initial cycle upon discharge and, possibly, due to weak interaction with the lithiated cPVac matrix, thus preventing Li₂S crystallization in the course of further reduction.

The chemical instability of carbonate-based electrolytes was already described by Kim et al.^[41] and also qualitatively confirmed by our model experiment, from which we conclude that electrolyte degradation might also happen in S40PVac-cathodes upon cyclization (Figure S12). It is very likely that the insufficient reduction of bound sulfur in S40PVac in contrast to S40PAN is a consequence of a higher nucleation barrier in nitrogen-free composites in contrast to nitrogen-containing composites in general. This phenomenon was explicitly described by Kaskel et al. for conventional S/C cathodes and confirmed by in situ XRD analysis.^[46] However, our study is the first to demonstrate that similar findings apply for composites with covalently attached sulfur and therefore deliver an important guideline for the synthesis of novel S/polymer composites. Based on these findings, a redox mechanism for S40PAN and S40PVac was proposed (Figure 9).

We propose, that the N-rich sites at the SPAN composite actively facilitate Li₂S crystallization, the latter being energetically less favored in the corresponding SPVac intermediates. Furthermore, a higher polarity of the carbon backbone in SPAN leads to higher polysulfide retention, whereas the carbon backbone in SPVac has a weaker interaction to such redox intermediates. Also, the thioamide groups in SPAN have been proposed to serve as additional docking sites for polysulfide reintegration upon charging (Figure S23).^[6a]

This underlines, that for the successful synthesis of S/polymer composites, a careful choice of potential precursor polymers is crucial. N-rich precursor polymers are likely to result

in more N-rich S/polymer composites after sulfuration and should be given more attention in this research field for novel active materials in metal-sulfur batteries.

Conclusion

Sulfurized poly(vinylacetylene) was successfully synthesized for the first time. Solid-state analyses revealed that sulfurated poly(vinylacetylene) (S40PVac) with molecular characteristics very similar to those of sulfurated poly(acrylonitrile) (S40PAN) is obtained. The preferable binding of short S_x-chains to the carbonaceous matrix, a very similar cyclization behavior at elevated temperatures and formation of an aromatic backbone was verified both in S40PVac and in S40PAN. Sulfur incorporation in PVac was more dependent on the applied temperature profile in comparison to PAN, especially below the onset of cyclization. Both in S40PVac- and S40PAN-based cathodes, a homogenous distribution of the S-containing composites along the cathode cross-sections was observed in the SEM-EDX images. Rate and cycle stability tests revealed a severe capacity decay in S40PVac in both, ether- and carbonate-based electrolytes, while S40PAN generates a cycle stable electrochemistry in carbonate-based electrolytes. We propose that the properties of S40PAN, which make this cathode material stand out of many others, are related to the presence of nitrogen in the carbonaceous matrix, leading to highly reversible redox chemistry. This study outlines both, the importance of covalent binding and the key role of a nitrogen-rich carbon backbone, which together allow for a reversible and highly rate capable electrochemistry.

Experimental Section/Methods

The synthesis of the herein used monomers, polymers, as well as the general procedures to obtain electrodes derived from S40PVac and S40PAN as well as all electrochemical methods are described in the Supporting Information.

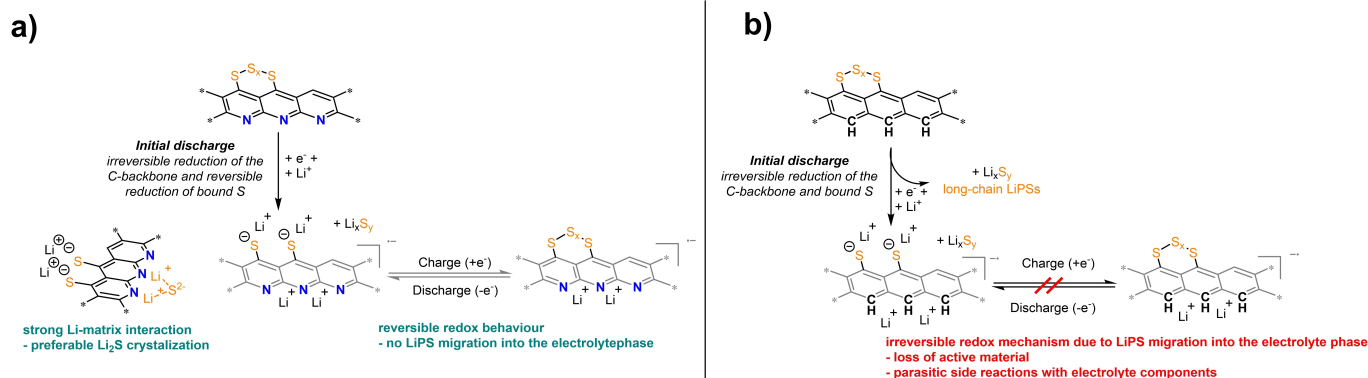


Figure 9. Postulated redox mechanisms of a) S40PAN and b) S40PVac in carbonate-based electrolytes according to our findings.

Acknowledgment

We thankfully acknowledge funding and support from the German Federal Ministry for Economic Affairs and Energy (BMW i, project no. S50400, FiMaLiS), the state of Baden-Württemberg through bwHPC and the German Research Foundation (DFG) through grant no. INST 40/575-1 FUGG (JUSTUS 2 cluster). Dr. Felix Ziegler is greatly acknowledged for help with the N₂-physisorption measurements; M.Sc. Jonas Groos is thanked for help with the ICP-OES measurements. We also want to thank Dipl.-Geol. Ulrich Hageroth and Dr. Marc Vocht, DITF Denkendorf, for help with SEM and TGA-MS measurements. Dr. Kathrin Küster is thanked for help concerning XPS measurements. Dr. Janis Musso, M.Sc. Stefan Niesen and Dr. Saravanakumar Murugan are thanked for fruitful discussions. Open Access funding enabled and organized by Projekt DEAL.

Conflict of Interest

The authors declare no conflict of interest.

Data Availability Statement

The data that support the findings of this study are available from the corresponding author upon reasonable request.

Keywords: lithium sulfur batteries · sulfurized poly(acrylonitrile) (SPAN) · poly(vinylacetylene) · N-containing polymers

- [1] a) F. Knobloch, S. Hanssen, A. Lam, H. Pollitt, P. Salas, U. Chewprecha, M. A. J. Huijbregts, J. F. Mercure, *Nat. Sustain.* **2020**, *3*, 437–447; b) J. W. Choi, D. Aurbach, *Nat. Rev. Mater.* **2016**, *1*.
- [2] P. G. Bruce, S. A. Freunberger, L. J. Hardwick, J.-M. Tarascon, *Nat. Mater.* **2011**, *11*, 19–29.
- [3] X. Ji, K. T. Lee, L. F. Nazar, *Nat. Mater.* **2009**, *8*, 500–506.
- [4] S. Li, B. Jin, X. Zhai, H. Li, Q. Jiang, *ChemistrySelect* **2018**, *3*, 2245–2260.
- [5] a) N. Kang, Y. Lin, L. Yang, D. Lu, J. Xiao, Y. Qi, M. Cai, *Nat. Commun.* **2019**, *10*; b) B. Zhang, M. Xiao, S. Wang, D. Han, S. Song, G. Chen, Y. Meng, *ACS Appl. Mater. Interfaces* **2014**, *6*, 13174–13182.
- [6] a) R. Mukkabl, M. R. Buchmeiser, *J. Mater. Chem. A* **2020**, *8*, 5379–5394; b) R. Fang, J. Xu, D.-W. Wang, *Energy Environ. Sci.* **2020**, *13*, 432–471.
- [7] a) J. Wang, J. Yang, J. Xie, N. Xu, *Adv. Mater.* **2002**, *14*, 963–965; b) X. Yu, J. Xie, J. Yang, K. Wang, *J. Power Sources* **2004**, *132*, 181–186.
- [8] a) J. Fanous, M. Wegner, J. Grimming, A. Andresen, M. R. Buchmeiser, *Chem. Mater.* **2011**, *23*, 5024–5028; b) J. Fanous, M. Wegner, J. Grimming, M. Rolff, M. B. M. Spera, M. Tenzer, M. R. Buchmeiser, *J. Mater. Chem.* **2012**, *22*, 23240; c) J. Fanous, M. Wegner, M. B. M. Spera, M. R. Buchmeiser, *J. Electrochem. Soc.* **2013**, *160*, A1169–A1170; d) C. J. Huang, K. Y. Lin, Y. C. Hsieh, W. N. Su, C. H. Wang, G. Bruncklaus, M. Winter, J. C. Jiang, B. J. Hwang, *ACS Appl. Mater. Interfaces* **2021**, *13*, 14230–14238.
- [9] a) S. Warneke, A. Hintennach, M. R. Buchmeiser, *J. Electrochem. Soc.* **2018**, *165*, A2093–A2095; b) S. Warneke, M. Eusterholz, R. K. Zenn, A. Hintennach, R. E. Dinnebie, M. R. Buchmeiser, *J. Electrochem. Soc.* **2017**, *165*, A6017–A6020.
- [10] T. Leberer, M. Frey, A. Hintennach, M. R. Buchmeiser, *RSC Adv.* **2019**, *9*, 7181–7188.
- [11] M. Frey, R. K. Zenn, S. Warneke, K. Müller, A. Hintennach, R. E. Dinnebie, M. R. Buchmeiser, *ACS Energy Lett.* **2017**, *2*, 595–604.
- [12] J. Lei, J. Chen, H. Zhang, A. Naveed, J. Yang, Y. Nuli, J. Wang, *ACS Appl. Mater. Interfaces* **2020**, *12*, 33702–33709.
- [13] X. Wang, Y. Qian, L. Wang, H. Yang, H. Li, Y. Zhao, T. Liu, *Adv. Funct. Mater.* **2019**, *29*, 1902929.
- [14] Y. Liu, W. Wang, A. Wang, Z. Jin, H. Zhao, Y. Yang, *RSC Adv.* **2016**, *6*, 106625–106630.
- [15] a) L. Wang, X. Chen, S. Li, J. Yang, Y. Sun, L. Peng, B. Shan, J. Xie, *J. Mater. Chem. A* **2019**, *7*, 12732–12739; b) Y. Zhang, Y. Sun, L. Peng, J. Yang, H. Jia, Z. Zhang, B. Shan, J. Xie, *Energy Storage Mater.* **2019**, *21*, 287–296; c) X. Chen, L. Peng, L. Wang, J. Yang, Z. Hao, J. Xiang, K. Yuan, Y. Huang, B. Shan, L. Yuan, J. Xie, *Nat. Commun.* **2019**, *10*, 1021.
- [16] S. Li, Z. Han, W. Hu, L. Peng, J. Yang, L. Wang, Y. Zhang, B. Shan, J. Xie, *Nano Energy* **2019**, *60*, 153–161.
- [17] S. Ma, Z. Zhang, Y. Wang, Z. Yu, C. Cui, M. He, H. Huo, G. Yin, P. Zuo, *Chem. Eng. J.* **2021**, *418*, 129410.
- [18] H. M. Kim, J.-Y. Hwang, D. Aurbach, Y.-K. Sun, *J. Phys. Chem. Lett.* **2017**, *8*, 5331–5337.
- [19] Q. Li, H. Yang, A. Naveed, C. Guo, J. Yang, Y. Nuli, J. Wang, *Energy Storage Mater.* **2018**, *14*, 75–81.
- [20] a) P. Wang, J. Kappler, B. Sievert, J. Häcker, K. Küster, U. Starke, F. Ziegler, M. R. Buchmeiser, *Electrochim. Acta* **2020**, *361*, 137024; b) P. Wang, K. Küster, U. Starke, C. Liang, R. Niewa, M. R. Buchmeiser, *J. Power Sources* **2021**, *515*, 230604; c) P. Wang, J. Trück, S. Niesen, J. Kappler, K. Küster, U. Starke, F. Ziegler, A. Hintennach, M. R. Buchmeiser, *Batteries & Supercaps* **2020**, *3*, 1239–1247; d) P. Wang, J. Trück, J. Häcker, A. Schlosser, K. Küster, U. Starke, L. Reinders, M. R. Buchmeiser, *Energy Storage Mater.* **2022**, *49*, 509–517.
- [21] a) S. Murugan, S. V. Klostermann, W. Frey, J. Kästner, M. R. Buchmeiser, *Electrochim. Commun.* **2021**, *132*, 107137; b) S. Murugan, S. V. Klostermann, P. Schützendübe, G. Richter, J. Kästner, M. R. Buchmeiser, *Adv. Funct. Mater.* **2022**, *32*, 2201191; c) S. Murugan, S. Niesen, J. Kappler, K. Küster, U. Starke, M. R. Buchmeiser, *Batteries & Supercaps* **2021**, *4*, 1636–1646.
- [22] J.-Y. Hwang, H. M. Kim, Y.-K. Sun, *J. Mater. Chem. A* **2018**, *6*, 14587–14593.
- [23] W. Wang, Z. Cao, G. A. Elia, Y. Wu, W. Wahyudi, E. Abou-Hamad, A.-H. Emwas, L. Cavallo, L.-J. Li, J. Ming, *ACS Energy Lett.* **2018**, *3*, 2899–2907.
- [24] X. Liu, Y. Makita, Y.-I. Hong, Y. Nishiyama, T. Miyoshi, *Macromolecules* **2016**, *50*, 244–253.
- [25] a) Z. Fu, B. Liu, L. Sun, H. Zhang, *Polym. Degrad. Stab.* **2017**, *140*, 104–113; b) J. Wang, L. Hu, C. Yang, W. Zhao, Y. Lu, *RSC Adv.* **2016**, *6*, 73404–73411.
- [26] A. Mavinkurve, S. Visser, A. J. Pennings, *Carbon* **1995**, *33*, 757–761.
- [27] J. H. Buehler, R. H. Freeman, R. G. Keister, M. P. McCready, B. I. Pesetsky, D. T. Watters, *Chem. Eng.* **1970**, *77*, 77.
- [28] a) Z. Chang, Y. Xu, X. Zhao, Q. Zhang, D. Chen, *ACS Appl. Mater. Interfaces* **2009**, *1*, 2804–2811; b) Q. Fengling, Y. Rongxing, W. Lianjun, L. Hongqi, M. Weidong, *e-Polym.* **2008**, *8*; c) L.-J. Wang, S. Liao, L.-Y. Wang, *Bull. Korean Chem. Soc.* **2011**, *32*, 1471–1474.
- [29] K. Krishnaveni, R. Subadevi, G. Radhika, T. Premkumar, M. Raja, W. R. Liu, M. Sivakumar, *J. Nanosci. Nanotechnol.* **2018**, *18*, 121–126.
- [30] a) Y. Jung, M. C. Suh, H. Lee, M. Kim, S. I. Lee, S. C. Shim, J. Kwak, *J. Electrochem. Soc.* **2019**, *144*, 4279–4284; b) S. Wei, L. Ma, K. E. Hendrickson, Z. Tu, L. A. Archer, *J. Am. Chem. Soc.* **2015**, *137*, 12143–12152.
- [31] a) W. J. Chung, J. J. Griebel, E. T. Kim, H. Yoon, A. G. Simmonds, H. J. Ji, P. T. Dirlam, R. S. Glass, J. J. Wie, N. A. Nguyen, B. W. Guralnick, J. Park, A. Somogyi, P. Theato, M. E. Mackay, Y. E. Sung, K. Char, J. Pyun, *Nat. Chem.* **2013**, *5*, 518–524; b) R. Steudel, B. Eckert, *Top. Curr. Chem.* **2003**, *230*, 1–80.
- [32] a) M. A. Pimenta, G. Dresselhaus, M. S. Dresselhaus, L. G. Cancado, A. Jorio, R. Saito, *Phys. Chem. Chem. Phys.* **2007**, *9*, 1276–1291; b) R. Kostecki, B. Schnyder, D. Allia, X. Song, K. Kinoshita, R. Kötz, *Thin Solid Films* **2001**, *396*, 36–43.
- [33] a) Y. Wang, B. Fugetsu, Z. Wang, W. Gong, I. Sakata, S. Morimoto, Y. Hashimoto, M. Endo, M. Dresselhaus, M. Terrones, *Sci. Rep.* **2017**, *7*, 40259; b) F. Xie, W. Hu, L. Ding, K. Tian, Z. Wu, L. Li, *Polym. Chem.* **2017**, *8*, 6106–6111.
- [34] a) R. A. A. F. Cordero, S. Cicchi, V. K. Aggarwal, *Science of Synthesis: Houben-Weyl Methods of Molecular Transformations* **2014**; b) D. D. D. Avilov, E. Block, J. Carretero, S. J. Collier, *Science of Synthesis: Houben-Weyl Methods of Molecular Transformations, Vol. 33*, **2014**.
- [35] a) M. Wahlqvist, A. Shchukarev, *J. Electron Spectrosc. Relat. Phenom.* **2007**, *156–158*, 310–314; b) Z. D. Hood, S. P. Adhikari, S. F. Evans, H. Wang, Y. Li, A. K. Naskar, M. Chi, A. Lachgar, M. P. Paranthaman, *Carbon*

- Resour. Convers.* **2018**, *1*, 165–173; c) S. K. Das, C. Dickinson, F. Lafir, D. F. Brougham, E. Marsili, *Green Chem.* **2012**, *14*, 1322.
- [36] Y. Zhang, R. S. Glass, K. Char, J. Pyun, *Polym. Chem.* **2019**, *10*, 4078–4105.
- [37] a) M. Müller, L. Pfaffmann, S. Jaiser, M. Baunach, V. Trouillet, F. Scheiba, P. Scharfer, W. Schabel, W. Bauer, *J. Power Sources* **2017**, *340*, 1–5; b) S. Niesen, J. Kappler, J. Truck, L. Veith, T. Weil, T. Soczka-Guth, M. R. Buchmeiser, *J. Electrochem. Soc.* **2021**, *168*, 050510.
- [38] a) A. Manthiram, Y. Fu, S. H. Chung, C. Zu, Y. S. Su, *Chem. Rev.* **2014**, *114*, 11751–11787; b) M. Wild, L. O'Neill, T. Zhang, R. Purkayastha, G. Minton, M. Marinescu, G. J. Offer, *Energy Environ. Sci.* **2015**, *8*, 3477–3494.
- [39] C.-J. Huang, J.-H. Cheng, W.-N. Su, P. Partovi-Azar, L.-Y. Kuo, M.-C. Tsai, M.-H. Lin, S. Panahian Jand, T.-S. Chan, N.-L. Wu, P. Kaghazchi, H. Dai, P. M. Bieker, B.-J. Hwang, *J. Power Sources* **2021**, *492*, 229508.
- [40] X. Li, M. Banis, A. Lushington, X. Yang, Q. Sun, Y. Zhao, C. Liu, Q. Li, B. Wang, W. Xiao, C. Wang, M. Li, J. Liang, R. Li, Y. Hu, L. Goncharova, H. Zhang, T. K. Sham, X. Sun, *Nat. Commun.* **2018**, *9*, 4509.
- [41] T. Yim, M.-S. Park, J.-S. Yu, K. J. Kim, K. Y. Im, J.-H. Kim, G. Jeong, Y. N. Jo, S.-G. Woo, K. S. Kang, I. Lee, Y.-J. Kim, *Electrochim. Acta* **2013**, *107*, 454–460.
- [42] a) M. Inagaki, M. Toyoda, Y. Soneda, T. Morishita, *Carbon* **2018**, *132*, 104–140; b) J. Wu, Z. Pan, Y. Zhang, B. Wang, H. Peng, *J. Mater. Chem. A* **2018**, *6*, 12932–12944.
- [43] A. Y. S. Eng, D.-T. Nguyen, V. Kumar, G. S. Subramanian, M.-F. Ng, Z. W. Seh, *J. Mater. Chem. A* **2020**, *8*, 22983–22997.
- [44] M. Fantauzzi, B. Elsener, D. Atzei, A. Rigoldi, A. Rossi, *RSC Adv.* **2015**, *5*, 75953–75963.
- [45] Z.-Q. Jin, Y.-G. Liu, W.-K. Wang, A.-B. Wang, B.-W. Hu, M. Shen, T. Gao, P.-C. Zhao, Y.-S. Yang, *Energy Storage Mater.* **2018**, *14*, 272–278.
- [46] S. Dörfler, P. Strubel, T. Jaumann, E. Troschke, F. Hippauf, C. Kensy, A. Schökel, H. Althues, L. Giebeler, S. Oswald, S. Kaskel, *Nano Energy* **2018**, *54*, 116–128.

Manuscript received: December 2, 2022

Revised manuscript received: January 3, 2023

Accepted manuscript online: January 5, 2023

Version of record online: January 18, 2023